# CD133 as a Biomarker for an Autoantibody-to-ImmunoPET Paradigm for the Early Detection of Small Cell Lung Cancer

Andrew G. Kunihiro*[1], Samantha M. Sarrett*[2–4], Kristin J. Lastwika*[1,5], Joell L. Solan[1], Tatyana Pisarenko[5], Outi Keinänen[2,4], Cindy Rodriguez[2–4], Lydia R. Taverne[1], Annette L. Fitzpatrick[6,7], Christopher I. Li[1], A. McGarry Houghton[5,8], Brian M. Zeglis[2–4,9], and Paul D. Lampe[1,8]

[1]*Translational Research Program, Public Health Sciences Division, Fred Hutchinson Cancer Research Center, Seattle, Washington;* [2]*Department of Chemistry, Hunter College, City University of New York, New York, New York;* [3]*Ph.D. Program in Biochemistry, City University of New York, New York, New York;* [4]*Department of Radiology, Memorial Sloan Kettering Cancer Center, New York, New York;* [5]*Clinical Research Division, Fred Hutchinson Cancer Research Center, Seattle, Washington;* [6]*Department of Family Medicine, University of Washington, Seattle, Washington;* [7]*Department of Global Health, University of Washington, Seattle, Washington;* [8]*Human Biology Division, Fred Hutchinson Cancer Research Center, Seattle, Washington; and* [9]*Department of Radiology, Weill Cornell Medical College, New York, New York*

Small cell lung cancer (SCLC) is a deadly neuroendocrine tumor for which there are no screening methods sensitive enough to facilitate early, effective intervention. We propose targeting the neuroendocrine tumor neoantigen CD133 via antibody-based early detection and PET (immunoPET) to facilitate earlier and more accurate detection of SCLC. **Methods:** RNA sequencing datasets, immunohistochemistry, flow cytometry, and Western blots were used to quantify CD133 expression in healthy and SCLC patients. CD133 was imaged *in vivo* using near-infrared fluorescence (NIRF) immunoimaging, and $^{89}$Zr immunoPET. Anti(α)-CD133 autoantibody levels were measured in SCLC patient plasma using antibody microarrays. **Results:** Across 6 publicly available datasets, CD133 messenger RNA was found to be higher in SCLC tumors than in other tissues, including healthy or normal adjacent lung and non-SCLC samples. Critically, the upregulation of CD133 messenger RNA in SCLC was associated with a significant increase (hazard ratio, 2.62) in death. CD133 protein was expressed in primary human SCLC, in SCLC patient-derived xenografts, and in both SCLC cell lines tested (H82 and H69). Using an H82 xenograft mouse model, we first imaged CD133 expression with NIRF. Both *in vivo* and *ex vivo* NIRF clearly showed that a fluorophore-tagged αCD133 homed to lung tumors. Next, we validated the noninvasive visualization of subcutaneous and orthotopic H82 xenografts via immunoPET. An αCD133 antibody labeled with the positron-emitting radiometal $^{89}$Zr demonstrated significant accumulation in tumor tissue while producing minimal uptake in healthy organs. Finally, plasma αCD133 autoantibodies were found in subjects from cohort studies up to 1 year before SCLC diagnosis. **Conclusion:** In light of these findings, we conclude that the presence of αCD133 autoantibodies in a blood sample followed by CD133-targeted $^{89}$Zr-immunoPET could be an effective early detection screening strategy for SCLC.

**Key Words:** SCLC; CD133; immunoPET; autoantibody

**J Nucl Med 2022; 63:1701–1707**
DOI: 10.2967/jnumed.121.263511

Most small cell lung cancer (SCLC) diagnoses are made at the extensive stage of the disease after metastases are widely distributed. Despite an initial response to etoposide and cisplatin, the median survival for extensive-stage SCLC is only 8–12 months. Although SCLC has a dismal 5-year survival rate of less than 3% for the extensive stage, this improves to nearly 50% if diagnosed at the limited stage, when treatments can be curative (*1,2*). Unfortunately, the annual low-dose CT recommended for heavy smokers (who comprise 90% of SCLC cases) is unreliable for detecting limited-stage SCLC (*1,3*). Other modalities, such as $^{18}$F-FDG PET, are also ineffective for identifying limited-stage disease (*4*). More advanced imaging methods—such as antibody-based PET (immunoPET)—offer higher specificity than $^{18}$F-FDG PET and increased spatial resolution compared with low-dose CT and could thus detect and locate even small SCLC lesions, allowing for effective therapeutic interventions (*5*).

CD133 is a glycoprotein expressed in many tumor types (including SCLC) that is often used as a marker for cancer stem cells (*6,7*). These cells, which have been imaged using an anti-CD133 monoclonal antibody–conjugated immunomagnetic nanosensor (*8*), are thought to drive tumor initiation, suggesting that CD133 upregulation occurs early in tumorigenesis and may thus be useful for early screening. CD133 is also associated with chemo- and radiotherapy resistance in SCLC cell lines and patient samples, indicating the functional relevance of its expression (*9,10*). Although CD133-positive tumors as small as 2 mm have been successfully imaged via immunoPET in preclinical models of cancers with poor prognoses (e.g., aggressive variant prostate cancer, colon cancer, and glioma), the utility of screening for SCLC by CD133-targeted immunoPET has yet to be explored (*6,11–13*).

Given the acute and unmet need for early detection of SCLC, this investigation focused on the creation of a novel diagnostic platform for the disease predicated on targeting CD133. To this end, we illustrated the feasibility of SCLC-specific imaging by comparing the expression of CD133 in healthy tissue versus SCLC and other lung tumors, performed near-infrared fluorescence (NIRF) and immunoPET imaging of CD133 in murine models of SCLC as a proof of concept for *in vivo* detection, and demonstrated that autoantibodies against CD133 are elevated a year before primary SCLC diagnosis but are not present in patients with colon cancer, pancreatic cancer,

Received Nov. 11, 2021; revision accepted Mar. 28, 2022.
For correspondence or reprints, contact Brian M. Zeglis (bz102@hunter.cuny.edu) or Paul D. Lampe (plampe@fredhutch.org).
*Contributed equally to this work.
Published online Apr. 28, 2022.

or non-SCLC. Ultimately, we propose that CD133 could form the basis of a noninvasive autoantibody-to-immunoPET paradigm that could be added to current lung cancer screening programs.

## MATERIALS AND METHODS

### CD133 Expression

Surface expression of CD133 was determined by flow cytometry: the human SCLC cell lines NCI-H82 and NCI-H69, purchased from ATCC, were incubated with a live/dead stain and then with anti-CD133 antibody (HB 7; Developmental Studies Hybridoma Bank) followed by anti-IgG-AF647 (A31571) and analyzed using a FACSCanto II (BD Bioscience).

Human tissue microarrays of healthy organs (FDA999-1, 33 organs per person from 3 persons; US Biolab) or SCLC cores (RLN681A, 62 unique cases [60 were of sufficient quality for evaluation] and 6 unique normal adjacent lung) were stained for CD133 (CST 64326) using the automated Bond RX system (Leica). Mouse lungs were formalin-fixed, paraffin-embedded, and sectioned onto glass slides. Adjacent sections were hematoxylin- and eosin-stained or imaged stain-free on an Odyssey CLx for αCD133-CF770.

SCLC RNA sequencing data were procured from the Gene Expression Omnibus and outlined in Supplemental Tables 1 and 2 (supplemental materials are available at http://jnm.snmjournals.org). Expression data and somatic mutations were also analyzed from the Cancer Cell Line Encyclopedia using the DepMap Public 21Q3 dataset or the SCLC patient sample as described in Supplemental Table 3 by George et al. (*14*).

### Small-Animal Imaging

All work was approved by local Institutional Animal Care and Use Committees and performed after anesthetization with a 2% isoflurane/oxygen mixture. Six-to-eight-week-old female athymic mice (JAX 007850 or 002019) were injected with 3–5 × $10^6$ H82 cells for flank xenografts. For orthotopic xenografts, 2–5 × $10^6$ H82 or H82-*luc* cells were percutaneously injected into the parenchyma of the left lung. The tumors reached an acceptable size for imaging and biodistribution studies (~50–100 $mm^3$) after 2–4 wk.

MRI was performed on a 1.0-T ICON system (Bruker BioSpin) running ParaVision (version 6.0.1) with image reconstruction in Osirix Lite (version 11.03). For NIRF imaging, mice bearing H82 tumors were injected retroorbitally with αCD133 monoclonal antibody (HB 7) conjugated to the near-infrared fluorophore CF770 (92222; Biotium)—αCD133-CF770 (50 μg)—3–4 wk after cell inoculation. NIRF imaging was performed up to 4 d after αCD133-CF770 injection, using an IVIS Spectrum with Living Image, version 4.7.2 (Perkin Elmer). Lungs were excised after terminal *in vivo* imaging and reimaged *ex vivo*.

PET images of the mice bearing subcutaneous xenografts were acquired using a microPET Focus 120 (Siemens Medical Solutions) (*15*). The mice underwent static scanning between 24 and 144 h after the intravenous tail vein administration of either [$^{89}$Zr]Zr-desferrioxamine (DFO)-αCD133 (3.7 − 3.9 MBq, 10–10.5 μg) or [$^{89}$Zr]Zr-DFO-$hIgG_1$ (3.3–3.5 MBq, 36–38 μg), for a total scan time of 10–30 min, with images analyzed using ASIPro VM (Concorde Microsystems). After terminal PET and euthanasia, the activity concentrations in 15 relevant organs were quantified using an $^{89}$Zr-calibrated Wizard$^2$ γ-counter (PerkinElmer).

### Autoantibody Microarrays

Autoantibody–antigen complexes were analyzed in SCLC patient plasma from the Cardiovascular Health Study (CHS; ancillary study 132) and the prostate, lung, colorectal, and ovarian (study 170) screening trial (*16–18*). We included 11 cases and 17 controls from CHS, and 20 SCLC cases with 38 controls from the prostate, lung, colorectal, and ovarian trial (Supplemental Table 3). Briefly, antibody microarrays were printed in-house, incubated with plasma, probed with antihuman IgG-SeTau647 or IgM-DyLight550 antibody, and imaged on a GenePix 4200A scanner with GenePix Pro, version 6.0 (Molecular Devices).

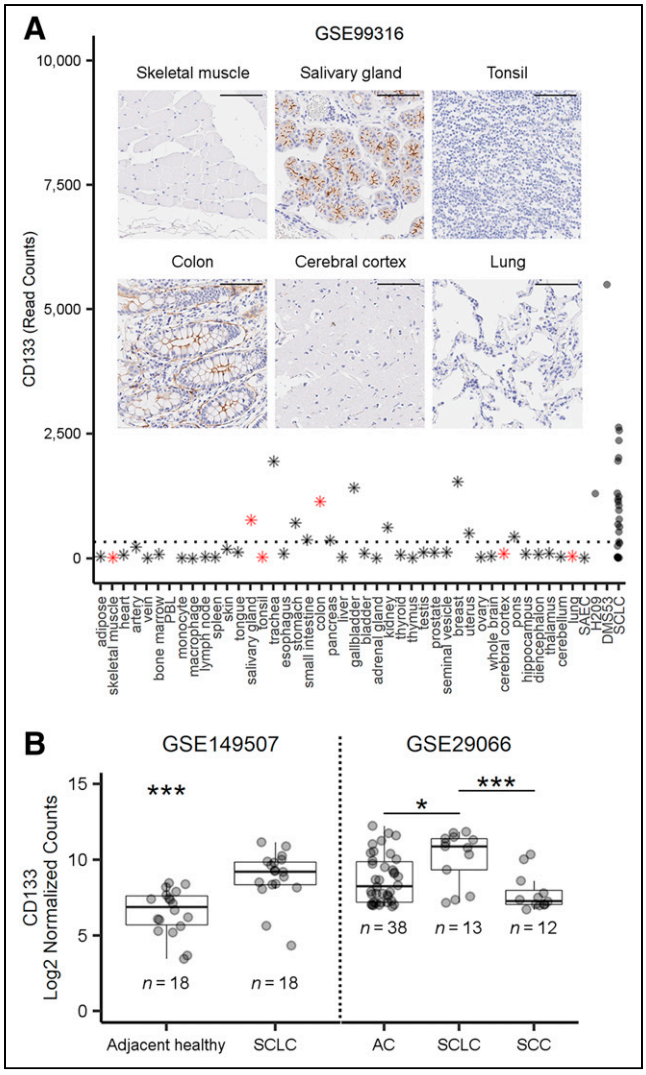


**FIGURE 1.** Expression of CD133 in normal tissue and SCLC. (A) RNA sequencing data for CD133 in healthy organs ($n$ = 42), SAEC ($n$ = 1), SCLC cell lines ($n$ = 2), and SCLC patient tumors ($n$ = 23). PBL = peripheral blood leukocytes; SAEC = small airway epithelial cell. Dashed line represents average expression across all healthy tissue/organs (exclusive of H209, DMS53, and SCLC). Inset shows CD133 protein immunohistochemistry staining (brown) at ×20 in tissue microarrays from selected normal tissues (red stars in A; scale, 100 μm). (B) Representative expression levels of CD133 messenger RNA, from publicly available cohorts, in adjacent healthy or tumor tissue from SCLC patients and between SCLC, adenocarcinoma (AC), and squamous cell carcinoma (SCC) tumors. *$P$ < 0.05 by $t$ test or 1-way ANOVA with Tukey adjustment. ***$P$ < 0.001 by $t$ test or 1-way ANOVA with Tukey adjustment.

### Statistics

Figures and statistics were prepared using RStudio (version 1.4.1717). When appropriate, $t$ tests or ANOVA with post hoc analyses were performed. Additional details can be found in the supplemental methods.

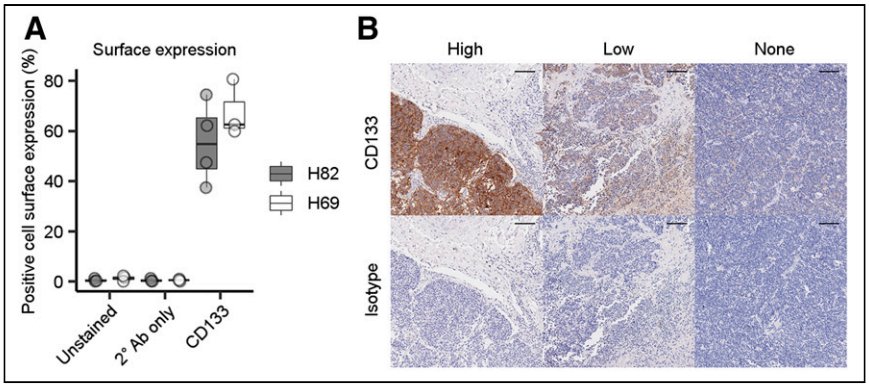


**FIGURE 2.** Characterization of expression of CD133 protein in SCLC. (A) Flow-cytometric detection of CD133 expression in H82 and H69 SCLC cell lines (4 experimental replicates per cell line). (B) Representative images of high, low, or absent CD133 expression (top; brown staining) or isotype control (bottom) from SCLC tissue microarray (scale, 100 μm).

## RESULTS

### CD133 Is Overexpressed in Limited-Stage SCLC Compared with Normal Tissues and Other Lung Tumors

Since the upregulation of CD133 has previously been reported in several tumor types but has not been uniquely examined in SCLC (*6,7,19*), we explored this relationship by analyzing publicly available RNA sequencing datasets. In a cohort of Japanese SCLC patients, the mean expression of CD133 was 5-fold higher than the mean expression across 43 organ samples (Fig. 1A and Supplemental Fig. 1B). CD133 expression was also elevated in H209 (4.7-fold) and DMS53 (20.2-fold) SCLC cell lines relative to other healthy tissues. Our immunohistochemical CD133 staining of a healthy-organ microarray showed high concordance between messenger RNA transcript levels and protein expression (Fig. 1A). Most normal tissues were negative for both CD133 messenger RNA and protein expression and thus are not expected to interfere with the imaging of lung tumors.

In a publicly available, commercially procured patient cohort (Supplemental Table 1), CD133 transcript levels were 2.64-fold greater in SCLC tumors than in normal lung tissue (Fig. 1B). On the basis of our analysis, CD133 was transcribed regardless of SCLC staging (Supplemental Figs. 1A and 2) and was higher in SCLC than in adenocarcinoma (3.34-fold) or squamous cell carcinoma (5.35-fold) (Fig. 1B). In 2 additional cohorts, we found CD133 to be 3.7 to 5.0-fold higher in SCLC tissue than in adjacent healthy tissue (Fig. 1B; Supplemental Fig. 1C). We also found that high CD133 transcript levels (6.34 mean log2 expression cut-point) were significantly associated with a 2.62-fold (95% CI, 1.03–6.69) increased risk of death in a cohort of Chinese SCLC patients (Supplemental Fig. 1D).

Flow cytometry confirmed that both SCLC cell lines expressed CD133 on the cell surface (Fig. 2A). Additionally, 2 of the 4 SCLC patient-derived xenografts displayed appreciable CD133 expression by immunoblotting (data not shown). In a tissue microarray containing cores from 60 SCLC cases and 6 normal adjacent lung tissues, CD133 was specifically expressed in 58% of the SCLC cores but not in any normal adjacent lung tissue, suggesting that *in vivo* imaging of CD133 focused on the lungs will have little background signal in normal lung tissue (representative stains in Fig. 2B). Finally, the expression of CD133 does not appear to be dependent on diagnostic stage, underscoring its potential for identifying limited-stage SCLC (Supplemental Fig. 2).

### CD133 Is Associated with ASCL1 and POU2F3 Subtypes

Although SCLC is historically categorized as a neuroendocrine tumor (ASCL1 or NEUROD1 expression), more recent classification approaches have also identified nonneuroendocrine (YAP1 or POU2F3 expression) lineages in a fraction (<20%) of SCLC tumors (*20*). A heat map comparing expression of CD133 and these 4 canonic SCLC molecular subtype markers was generated from publicly available data (Fig. 3). CD133 expression was localized primarily in the ASCL1-positive cluster (SCLC-A)—the largest cluster identified (61/149)—and ASCL1 was the primary driver of CD133 expression (Supplemental Figs. 3 and 4). The other neuroendocrine cluster, NEUROD1-positive (SCLC-N, 28/149), did not have high levels of CD133 expression. Interestingly, a CD133- and POU2F3-positive cluster (SCLC-P, 36/149) suggested that CD133 may also be useful for identifying a nonneuroendocrine subtype of SCLC. YAP1–positive SCLC (SCLC-Y, 24/149) did not have high levels of CD133 expression. Taken together, these data underscore the utility of using CD133 to identify most cases of SCLC, including both neuroendocrine and nonneuroendocrine subtypes.

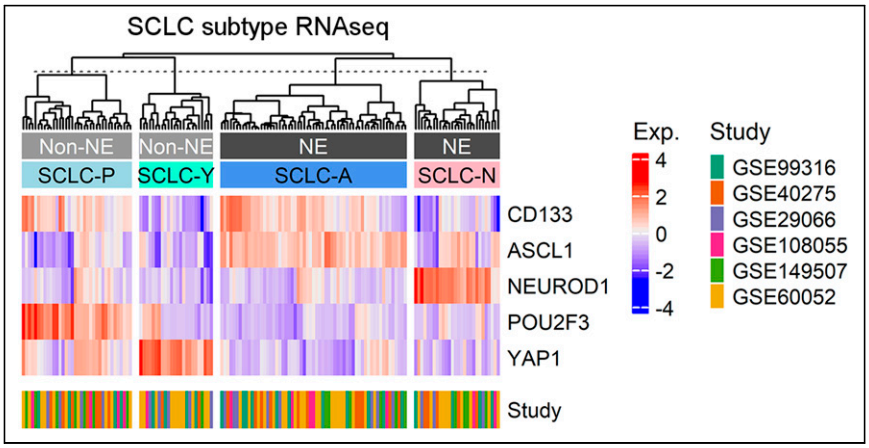


**FIGURE 3.** Clustering of CD133 expression and subtype markers in SCLC. RNA sequencing data from SCLC Gene Expression Omnibus data were used to construct heat map of CD133 and SCLC subtype marker expression using ComplexHeatmap R package with clustering using Ward.D2 method. *z* score of expression was calculated using scale function in R. Clusters are labeled by their characteristics (neuroendocrine [NE] or nonneuroendocrine [non-NE]) and by subtype (SCLC-A/N/P/Y). RNAseq = RNA sequencing.

### A Fluorophore-Tagged αCD133 Antibody Can Identify Both Subcutaneous and Orthotopic SCLC Tumors *In Vivo*

Using NIRF imaging, we demonstrated that an αCD133 antibody labeled with a near-infrared fluorophore—αCD133-CF770—effectively delineated subcutaneous H82

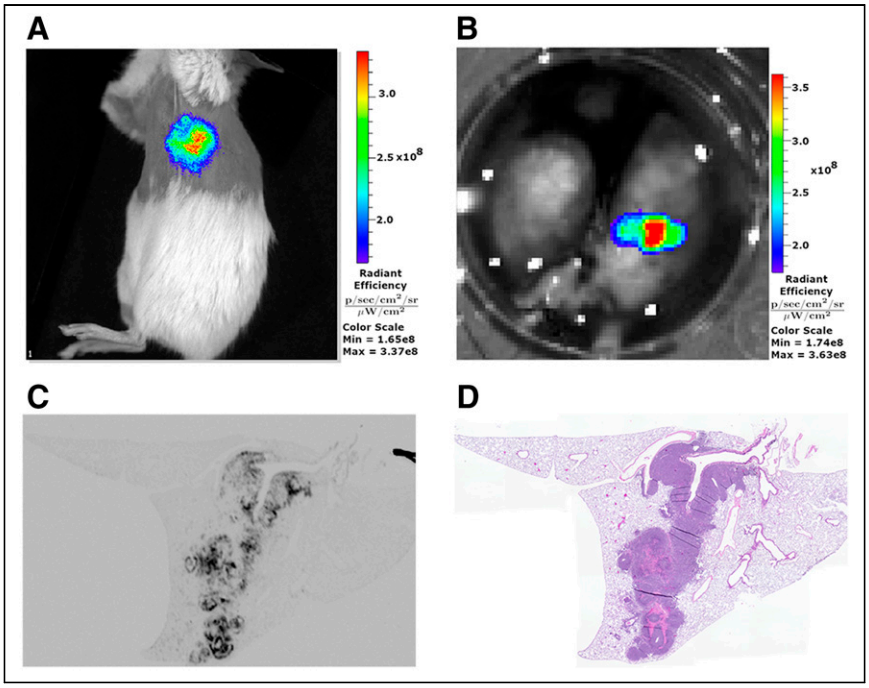


**FIGURE 4.** NIRF imaging of CD133 in SCLC. (A) Representative *in vivo* NIRF imaging of orthotopic H82 lung tumor in female NSG mouse after administration of αCD133-CF770. (B) *Ex vivo* NIRF imaging of excised lungs from mouse in A. (C and D) NIRF (C) and hematoxylin and eosin (D) imaging of adjacent histologic sections from same lung shown in A and B.

flank xenografts in female Fox1$^{nu}$ nude and NSG mice (Supplemental Figs. 5A–5C). NSG mice were also inoculated with H82 cells in the left lobe of the lung to form orthotopic tumors (Supplemental Figs. 5D–5F). After 2–4 wk, these orthotopic tumors were imaged via αCD133-CF770 NIRF imaging, producing visible signal emanating from the left lung (Fig. 4A; Supplemental Fig. 5G). At the end of the experiment, the lungs were harvested and *ex vivo* NIRF imaging confirmed that the signal was derived from the orthotopic, left-lobe tumor (Fig. 4B). After the histologic processing of the lung, *ex vivo* NIRF imaging of adjacent sections (Fig. 4C) confirmed tumor growth in the left lobe that colocalized with hematoxylin and eosin staining (Fig. 4D), confirming that the *in vivo* NIRF signal was from the orthotopic tumor.

### SCLC Tumors Can Be Delineated via ImmunoPET Using $^{89}$Zr-Labeled αCD133

Having illustrated the feasibility of visualizing CD133 expression *in vivo* using immunoNIRF, we next turned to the creation of a more clinically relevant immunoPET probe. To this end, the same αCD133 monoclonal antibody was modified with the chelator DFO via the stochastic ligation of *p*-SCN-Bn-DFO to the lysines of the immunoglobulin (Supplemental Fig. 6). Matrix-assisted laser desorption/ionization time-of-flight spectrometry revealed that the resulting immunoconjugate—DFO-αCD133—boasted a degree of labeling of 2.2 ± 0.4 DFO/monoclonal antibody (Supplemental Fig. 7). DFO-αCD133 was then radiolabeled with the positron-emitting radiometal $^{89}$Zr (half-life, 3.3 d) to create a radioimmunoconjugate, [$^{89}$Zr]Zr-DFO-αCD133, in more than 99% radiochemical purity that remained more than 95% intact in human serum over 5 d at 37°C (Supplemental Fig. 8). An immunoreactivity assay with CD133-expressing H82 human SCLC cells revealed that the radioimmunoconjugate boasted an immunoreactive fraction of more than 0.75. In contrast, a complementary immunoreactivity assay with CD133-negative K562 cells clearly demonstrated that the radioimmunoconjugate did not bind cells in the absence of its target antigen (Supplemental Fig. 9) (*21*).

With these radioimmunoconjugates in hand, we next evaluated their *in vivo* behavior in a xenograft mouse model of SCLC. To this end, female athymic nude mice bearing subcutaneous flank H82 tumors were administered [$^{89}$Zr]Zr-DFO-αCD133 (3.7 − 3.9 MBq, 10–10.5 μg) or [$^{89}$Zr] Zr-DFO-hIgG$_1$ (3.3–3.5 MBq, 36–38 μg) via intravenous tail-vein injection. The *in vivo* behavior of these radioimmunoconjugates was then assessed via the acquisition of static PET images 24, 72, 120, and 144 h after intravenous administration. The images clearly showed the accumulation of radioactivity signal in the tumor tissue over time, with the tumoral activity concentrations reaching more than 40 percentage injected dose (%ID)/g (Fig. 5A; Supplemental Fig. 10; Supplemental Table 4). A concomitant decrease in signal was observed in all healthy organs over the course of the experiments, ultimately leading to images with very high tumor-to-background contrast.

A terminal biodistribution analysis was performed after the final imaging time point to quantify the uptake of [$^{89}$Zr]Zr-DFO-αCD133 and compare it with that of [$^{89}$Zr]Zr-DFO-hIgG$_1$ (Fig. 5B; Supplemental Table 5). These data largely mirrored the PET data. A stark difference in the tumoral activity concentrations of the 2 radioimmunoconjugates was observed: 50.8 ± 7.7 %ID/g for [$^{89}$Zr]Zr-DFO-αCD133 and 5.8 ± 4.0 %ID/g for [$^{89}$Zr]Zr-DFO-hIgG$_1$, reinforcing the specificity of the former. Most healthy tissues displayed less than 5 %ID/g of [$^{89}$Zr]Zr-DFO-αCD133, with only the blood (10.1 ± 1.9 %ID/g) presenting a value above this level at 144 h after injection. Both the imaging and the biodistribution data demonstrated very low accretion in the tissues normally associated with metabolism and clearance of $^{89}$Zr-labeled radioimmunoconjugates: the liver, spleen, and bone. Finally, PET imaging experiments on mice bearing orthotopic H82-*luc* SCLC xenografts in the parenchyma of the left lung yielded promising results as well (Fig. 5C; Supplemental Fig. 11). The radioimmunoconjugate clearly visualized the tumor tissue and provided images with high tumor-to-background (and especially tumor–to–healthy-lung) contrast. Autoradiography of the left (tumor-bearing) and right (healthy) lungs underscored the dramatic difference in radioactivity in each tissue (Fig. 5D).

### αCD133 Autoantibodies Are Upregulated in Plasma up to 1 Year Before Diagnosis of SCLC

Though we have clearly demonstrated the utility of CD133 as a target for SCLC imaging, several factors (including cost, equipment availability, and radiation exposure) limit the feasibility of diagnostic PET scans for all patients at risk of developing SCLC. Therefore, we posited that a blood-based assay to screen high-risk individuals for CD133 would be necessary for the realistic clinical implementation of CD133-targeted immunoPET in SCLC patients. Antitumor autoantibodies—such as those resulting in paraneoplastic syndromes (*22*)—can be elevated during the very early stages of cancer,

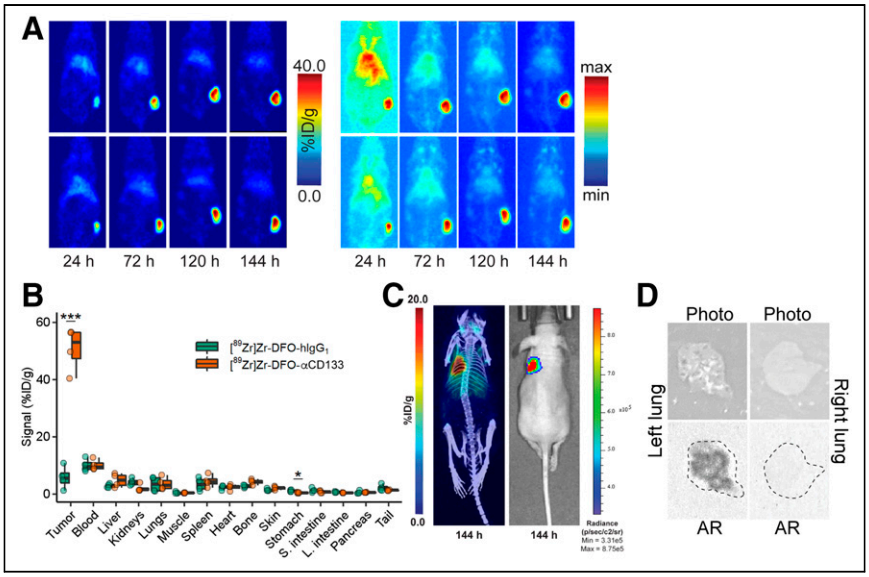


**FIGURE 5.** *In vivo* validation of [$^{89}$Zr]Zr-DFO-αCD133. (A) Representative coronal slice (left) and maximum-intensity-projection (right) PET images acquired 24, 72, 120, and 144 h after intravenous administration of [$^{89}$Zr]Zr-DFO-αCD133 (3.7 − 3.9 MBq, 10–10.5 μg) to athymic nude mice ($n$ = 4) bearing subcutaneous H82 xenografts (150–200 mm$^3$ at time of injection). For maximum-intensity-projection images, minimum is 0% and maximum is 100%. (B) Biodistribution data acquired 144 h after intravenous administration of [$^{89}$Zr]Zr-DFO-αCD133 (3.7–3.9 MBq, 10.0–10.5 μg) or [$^{89}$Zr]Zr-DFO-hIgG1 (3.3–3.5 MBq, 36–38 μg) to athymic nude mice ($n$ = 4 per cohort) bearing subcutaneous H82 xenografts. *$P$ < 0.05 using 2-way ANOVA and Bonferroni adjustment. ***$P$ < 0.0001 using 2-way ANOVA and Bonferroni adjustment. (C) Representative maximum-intensity-projection PET/CT (left) and bioluminescence images (right) acquired 144 h after intravenous administration of [$^{89}$Zr]Zr-DFO-αCD133 (3.7 − 3.9 MBq, 5–5.5 μg) to athymic nude mice ($n$ = 4) bearing orthotopic H82-*luc* xenografts in parenchyma of left lung. (D) White-light images and autoradiographs of left and right lungs of mouse shown in C; dotted lines in autoradiographs represent outline of lung.

sometimes even preceding clinical diagnoses by many months or years (*23*). We therefore determined the presence of αCD133 autoantibody–antigen complexes in the plasma of patients later diagnosed with SCLC within 1 year of a blood draw as well as controls matched by age, sex, and smoking status (i.e., case-control design) from the CHS and prostate, lung, colorectal, and ovarian cohorts. In both cohorts, those later diagnosed with SCLC were significantly more likely than controls to have circulating autoantibodies bound to CD133 (Fig. 6). Given that subject samples were drawn at different times before SCLC diagnosis, we measured both early-response IgM and later-produced IgG isotypes. Using a standardized log2 odds ratio cutoff (0.73) that maximized sensitivity and specificity, we found that 5 SCLC cases had both IgG and IgM autoantibodies, 8 had only IgM, 7 had only IgG, and 11 (35%) had no αCD133 autoantibodies (data not shown), yielding an overall sensitivity of 65% at 71% specificity. Importantly, αCD133 autoantibodies were elevated in SCLC but not in the other tumors we have tested (e.g., colon, pancreas, and non-SCLC) (Supplemental Fig. 12).

## DISCUSSION

Although heavy smokers already fall within the lung cancer screening guidelines, a retrospective analysis of the National Lung Screening Trial showed that only 34% of SCLC cases were detected by a scheduled screen. Moreover, stage I/II cancers—for which therapies are most effective—were only discovered with very small nodules (3–7 mm), which unfortunately comprised only 15% of all those detected by the screening (~85% were at more advanced stages). In contrast, all nodules measuring at least 7 mm had already progressed to stage III/IV (*5*). A search of the literature uncovered only 4 imaging agents for SCLC currently in development, with none being leveraged as screening tools (*24–28*). Yet the identification of highest-risk populations within those already attending annual lung cancer screens as candidates for noninvasive molecular imaging could help detect smaller, treatable tumors. In this study, we have identified CD133 as a novel antigen that is upregulated even in limited-stage SCLC and have developed a CD133-targeted $^{89}$Zr-immunoPET probe that can delineate tumor tissue with high contrast in murine models of SCLC.

We found that CD133 consistently correlated with ASCL1 and POU2F3 but not with YAP1 or NEUROD1 molecular subtypes of lung cancer. This finding aligns with a prior report that ASCL1 can transcriptionally regulate CD133 expression and increase tumorigenicity in SCLC cells and mouse xenograft models (*29*). However, to our knowledge, this is the first report of an association between CD133 and POU2F3 in SCLC. Because POU2F3 is a master regulator of tuft cells (*30*) and ASCL1 drives neuroendocrine cells, CD133 may be useful for the detection of both neuroendocrine and nonneuroendocrine SCLC. Overall, we found CD133 expression at the transcript and protein levels in approximately 60% of SCLC cases examined. Interestingly, our αCD133 autoantibody biomarkers mirror this prevalence with a sensitivity of 65%. Current research is ongoing to identify additional autoantibodies or markers needed to capture all SCLC cases.

Although CD133 is expressed in other types of cancer, we do not believe that this would interfere with CD133-targeted SCLC imaging because (i) immunoPET would be triggered only after αCD133 autoantibodies were detected by blood assay, indicating SCLC is present, and (ii) αCD133 autoantibodies are not elevated in major cancers (Supplemental Fig. 12). The case for CD133-targeted immunoPET in SCLC is strengthened by the low levels of CD133 expression in healthy thoracic organs (e.g., the lungs, heart, and thymus), suggesting that PET focused on the lungs and mediastinal region should allow for the effective spatial resolution of early intrathoracic tumors for which therapeutic interventions are possible. Importantly, *in vivo* blocking of [$^{89}$Zr]Zr-DFO-αCD133 by endogenous autoantibodies is unlikely, as we did not detect human IgG in a tissue microarray containing 45 SCLC tumors (Supplemental Fig. 13) but did see extensive staining of SCLC tissue with the αCD133 antibody (Fig. 2). Finally, the shedding of CD133 is unlikely to impede its viability as an imaging target, as $^{89}$Zr-immunoPET probes against several shed antigens—most notably VEGF-A and CA19.9—have been effectively deployed in the clinic (*31,32*).

Although the goal of this study was to assess CD133 as a target for early SCLC detection via immunoimaging, CD133 may also serve as a therapeutic target. Indeed, the presence of autoantibodies in prediagnostic cohorts of SCLC argues that CD133 may be a good target for early intervention with immunotherapy. In fact, αCD133

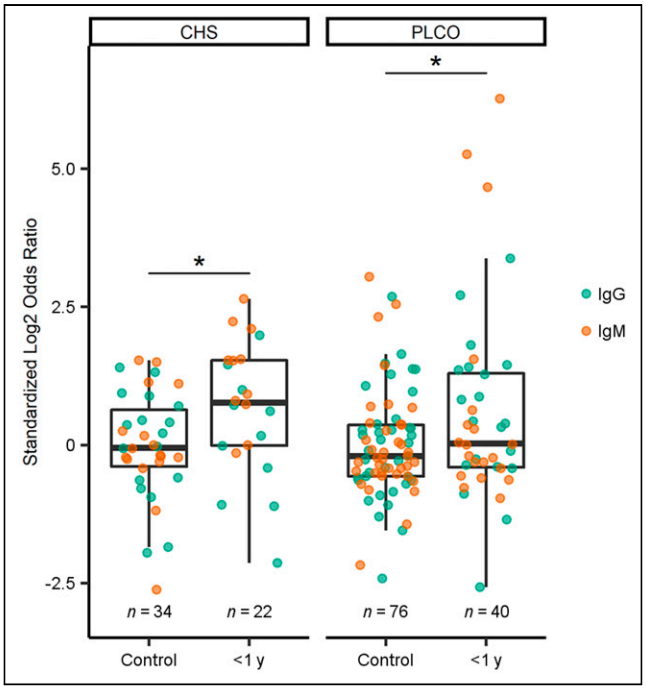


**FIGURE 6.** Expression of αCD133 autoantibodies in plasma of healthy controls or SCLC patients in 2 prediagnostic cohorts from CHS and prostate, lung, colorectal, and ovarian screening trial. *$P < 0.05$ using 2-way ANOVA and Bonferroni adjustment. PLCO = prostate, lung, colorectal, and ovarian.

immunotherapies and antibody–drug conjugates have shown promise for increasing survival in preclinical models of glioma and myeloid leukemia as well as colorectal, hepatocellular, and gastric cancers (*33–38*). Phase I/II human trials of αCD133 chimeric antigen receptor T cells have also shown improvements in remission or stable disease for an array of malignancies (*39–41*).

## CONCLUSION

We have clearly demonstrated the increased transcription of CD133 messenger RNA in SCLC tumors and the overexpression of CD133 protein in SCLC cell lines, patient-derived xenografts, and primary tumor samples. In addition, we have shown that CD133-targeted molecular imaging probes can delineate SCLC xenografts via both NIRF and immunoPET. Finally, we discovered that elevated levels of IgM and IgG autoantibodies against CD133 are present in the blood of SCLC patients up to a year before diagnosis. Supported by these data, we envision the creation of a novel 2-tiered αCD133 autoantibody-to-immunoPET early detection paradigm in which a plasma-based biomarker could serve as a companion diagnostic to select patients for noninvasive molecular imaging of SCLC.

## DISCLOSURE

This study was supported by the NIH (P50CA228944, R01CA243328, R01CA186157, and U01CA185097 to Paul Lampe and A. McGarry Houghton; R01CA240963, U01CA221046, R01CA204167, R21EB030275, R01CA244327 to Brian Zeglis; F32CA261055 and T32CA009657 to Andrew Kunihiro; KL2TR002317 to Kristin Lastwika; R25GM086304 supporting Lydia Taverne; and P30CA015704 to the FHCRC/UW Cancer Consortium) and the Academy of Finland (331659 to Outi Keinänen). CHS samples were used with support from HHSN268201200036C, HHSN268200800007C, HHSN268201800001C, N01HC55222, N01HC85079, N01HC85080, N01HC85081, N01HC85082, N01HC85083, N01HC85086, 75N92021D00006, U01HL080295, and U01HL130114 from the NHLBI; additional contributions from the NINDS; and R01AG023629 from the NIA. A full list of principal CHS investigators and institutions can be found at CHS-NHLBI.org. No other potential conflict of interest relevant to this article was reported.

**KEY POINTS**

**QUESTION:** Is CD133 a promising biomarker for the early detection and diagnostic immunoPET of SCLC?

**PERTINENT FINDINGS:** CD133 messenger RNA and protein levels are elevated in SCLC tumors, and autoantibodies against CD133 are present in SCLC patients up to a year before diagnosis. ImmunoPET with a $^{89}$Zr-labeled CD133-targeted radioimmunoconjugate effectively delineates SCLC tissue in murine models of the disease.

**IMPLICATIONS FOR PATIENT CARE:** The development of a CD133-targeted early detection and imaging strategy for SCLC will help identify high-risk patients with limited-stage disease and thus facilitate early therapeutic interventions.

## REFERENCES

1. Wang S, Zimmermann S, Parikh K, Mansfield AS, Adjei AA. Current diagnosis and management of small-cell lung cancer. *Mayo Clin Proc.* 2019;94:1599–1622.
2. Howlader N, Noone AM, Krapcho M, et al. (eds). SEER Cancer Statistics Review, 1975-2016, National Cancer Institute. Bethesda, MD, https://seer.cancer.gov/csr/1975_2016/, based on November 2018 SEER data submission, posted to the SEER website, April 2019. Accessed October 4, 2022.
3. Aberle DR, Adams AM, Berg CD; The National Lung Screening Trial Research Team. Reduced lung-cancer mortality with low-dose computed tomographic screening. *N Engl J Med.* 2011;365:395–409.
4. Van't Westeinde SC, De Koning HJ, Thunnissen FB, et al. The role of the $^{18}$F-fluorodeoxyglucose-positron emission tomography scan in the Nederlands Leuvens Longkanker Screenings Onderzoek lung cancer screening trial. *J Thorac Oncol.* 2011;6:1704–1712.
5. Thomas A, Pattanayak P, Szabo E, Pinsky P. Characteristics and outcomes of small cell lung cancer detected by CT screening. *Chest.* 2018;154:1284–1290.
6. Glumac PM, Gallant JP, Shapovalova M, et al. Exploitation of CD133 for the targeted imaging of lethal prostate cancer. *Clin Cancer Res.* 2020;26:1054–1064.
7. Qiu ZX, Zhao S, Mo X-m, Li W-m. Overexpression of PROM1 (CD133) confers poor prognosis in non-small cell lung cancer. *Int J Clin Exp Pathol.* 2015;8:6589–6595.
8. Wang X, Li B, Li R, et al. Anti-CD133 monoclonal antibody conjugated immunomagnetic nanosensor for molecular imaging of targeted cancer stem cells. *Sens Actuators B Chem.* 2018;255:3447–3457.
9. Yang K, Zhao Y, Du Y, Tang R. Evaluation of Hippo pathway and CD133 in radiation resistance in small-cell lung cancer. *J Oncol.* 2021;2021:8842554.
10. Kubo T, Takigawa N, Osawa M, et al. Subpopulation of small-cell lung cancer cells expressing CD133 and CD87 show resistance to chemotherapy. *Cancer Sci.* 2013;104:78–84.
11. Tsurumi C, Esser N, Firat E, et al. Non-invasive *in vivo* imaging of tumor-associated CD133/prominin. *PLoS One.* 2010;5:e15605.
12. Gaedicke S, Braun F, Prasad S, et al. Noninvasive positron emission tomography and fluorescence imaging of CD133+ tumor stem cells. *Proc Natl Acad Sci USA.* 2014;111:E692–E701.
13. Liu Y, Yao X, Wang C, et al. Peptide-based $^{68}$Ga-PET radiotracer for imaging CD133 expression in colorectal cancer. *Nucl Med Commun.* 2021;42:1144–1150.
14. George J, Lim JS, Jang SJ, et al. Comprehensive genomic profiles of small cell lung cancer. *Nature.* 2015;524:47–53.

15. Fung K, Vivier D, Keinänen O, Sarbisheh EK, Price EW, Zeglis BM. $^{89}$Zr-labeled AR20.5: a MUC1-targeting immunoPET probe. *Molecules.* 2020;25:1–13.
16. Rho JH, Lampe PD. High-throughput screening for native autoantigen-autoantibody complexes using antibody microarrays. *J Proteome Res.* 2013;12:2311–2320.
17. Hocking WG, Hu P, Oken MM, et al. Lung cancer screening in the randomized prostate, lung, colorectal, and ovarian (PLCO) cancer screening trial. *J Natl Cancer Inst.* 2010;102:722–731.
18. Rho JH, Ladd JJ, Li CI, et al. Protein and glycomic plasma markers for early detection of adenoma and colon cancer. *Gut.* 2018;67:473–484.
19. Mia-Jan K, Munkhdelger J, Lee MR, et al. Expression of CD133 in neuroendocrine neoplasms of the digestive tract: a detailed immunohistochemical analysis. *Tohoku J Exp Med.* 2013;229:301–309.
20. Rudin CM, Poirier JT, Byers LA, et al. Molecular subtypes of small cell lung cancer: a synthesis of human and mouse model data. *Nat Rev Cancer.* 2019;19:289–297.
21. Cui XY, Skretting G, Jing Y, Sun H, Sandset PM, Sun L. Hypoxia influences stem cell-like properties in multidrug resistant K562 leukemic cells. *Blood Cells Mol Dis.* 2013;51:177–184.
22. Gandhi L, Johnson BE. Paraneoplastic syndromes associated with small cell lung cancer. *J Natl Compr Canc Netw.* 2006;4:631–638.
23. Zaenker P, Gray ES, Ziman MR. Autoantibody production in cancer: the humoral immune response toward autologous antigens in cancer patients. *Autoimmun Rev.* 2016;15:477–483.
24. Johnson ML, Zvirbule Z, Laktionov K, et al. Rovalpituzumab tesirine as a maintenance therapy after first-line platinum-based chemotherapy in patients with extensive-stage–SCLC: results from the phase 3 MERU study. *J Thorac Oncol.* 2021;16:1570–1581.
25. Krug LM, Milton DT, Jungbluth AA, et al. Targeting Lewis Y (Le$^{y}$) in small cell lung cancer with a humanized monoclonal antibody, hu3S193: a pilot trial testing two dose levels. *J Thorac Oncol.* 2007;2:947–952.
26. Kwekkeboom DJ, Kam BL, Van Essen M, et al. Somatostatin receptor-based imaging and therapy of gastroenteropancreatic neuroendocrine tumors. *Endocr Relat Cancer.* 2010;17:R53–R73.
27. Zhou J, Chen J, Mokotoff M, Zhong R, Shultz LD, Ball ED. Bombesin/gastrin-releasing peptide receptor: a potential target for antibody-mediated therapy of small cell lung cancer. *Clin Cancer Res.* 2003;9:4953–4960.
28. Quaia E, Krug LM, Pandit-Taskar N, et al. The value of gamma camera and computed tomography data set coregistration to assess Lewis Y antigen targeting in small cell lung cancer by $^{111}$indium-labeled humanized monoclonal antibody 3S193. *Eur J Radiol.* 2008;67:292–299.
29. Jiang T, Collins BJ, Jin N, et al. Achaete-scute complex homologue 1 regulates tumor-initiating capacity in human small cell lung cancer. *Cancer Res.* 2009;69:845–854.
30. Huang YH, Klingbeil O, He XY, et al. POU2F3 is a master regulator of a tuft cell-like variant of small cell lung cancer. *Genes Dev.* 2018;32:915–928.
31. Lohrmann C, O'Reilly EM, O'Donoghue JA, et al. Retooling a blood-based biomarker: phase I assessment of the high-affinity CA19-9 antibody HuMab-5B1 for immunoPET imaging of pancreatic cancer. *Clin Cancer Res.* 2019;25:7014–7023.
32. Jansen MH, Lagerweij T, Sewing AC, et al. Bevacizumab targeting diffuse intrinsic pontine glioma: results of $^{89}$Zr-bevacizumab PET imaging in brain tumor models. *Mol Cancer Ther.* 2016;15:2166–2174.
33. Koerner SP, André MC, Leibold JS, et al. An Fc-optimized CD133 antibody for induction of NK cell reactivity against myeloid leukemia. *Leukemia.* 2017;31:459–469.
34. Hu B, Zou Y, Zhang L, et al. Nucleofection with plasmid DNA for CRISPR/Cas9-mediated inactivation of programmed cell death protein 1 in CD133-specific CAR T cells. *Hum Gene Ther.* 2019;30:446–458.
35. Prasad S, Gaedicke S, Machein M, et al. Effective eradication of glioblastoma stem cells by local application of an AC133/CD133-specific T-cell-engaging antibody and CD8 T cells. *Cancer Res.* 2015;75:2166–2176.
36. Smith LM, Nesterova A, Ryan MC, et al. CD133/prominin-1 is a potential therapeutic target for antibody-drug conjugates in hepatocellular and gastric cancers. *Br J Cancer.* 2008;99:100–109.
37. Zhao L, Yang Y, Zhou P, et al. Targeting CD133 high colorectal cancer cells *in vitro* and *in vivo* with an asymmetric bispecific antibody. *J Immunother.* 2015;38:217–228.
38. Zhu X, Prasad S, Gaedicke S, Hettich M, Firat E, Niedermann G. Patient-derived glioblastoma stem cells are killed by CD133-specific CAR T cells but induce the T cell aging marker CD57. *Oncotarget.* 2015;6:171–184.
39. Wang Y, Chen M, Wu Z, et al. CD133-directed CAR T cells for advanced metastasis malignancies: a phase I trial. *OncoImmunology.* 2018;7:e1440169.
40. Feng KC, Guo Y-L, Liu Y, et al. Cocktail treatment with EGFR-specific and CD133-specific chimeric antigen receptor-modified T cells in a patient with advanced cholangiocarcinoma. *J Hematol Oncol.* 2017;10:4.
41. Dai H, Tong C, Shi D, et al. Efficacy and biomarker analysis of CD133-directed CAR T cells in advanced hepatocellular carcinoma: a single-arm, open-label, phase II trial. *OncoImmunology.* 2020;9:1846926.